13th World Conference on Earthquake Engineering
Vancouver, B.C., Canada
August 1-6, 2004
Paper No. 1002

BRIDGE ISOLATION WITH HIGH-DAMPING RUBBER BEARINGS – ANALYTICAL MODELLING AND SYSTEM RESPONSE

Damian N. GRANT[1], Gregory L. FENVES[2] and Ferdinando AURICCHIO[3]

SUMMARY

High-damping rubber (HDR) bearings are used in seismic isolation applications for buildings and bridges, although no models are currently available for the accurate description of the shear force–deformation response under bidirectional loading. A strain rate-independent, phenomenological model is presented which effectively represents the stiffness and damping of HDR bearings for a range of shear strains. The model decomposes the resisting force vector as the sum of an elastic component, obtained from a generalised Mooney–Rivlin strain energy function, and a hysteretic force, described by an approach similar to bounding surface plasticity. The proposed model is used in a series of parametric studies of isolated bridge systems with ground motion of varying intensity. It is found that, while the HDR bearing system is effective at design levels of earthquake intensity, at higher levels of ground motion, significant inelastic demand may be experienced in bridge piers. Capacity design philosophy, which requires a ductile failure mechanism for any level of earthquake intensity, implies that ductility must be provided in the piers, and the interaction between pier yielding and bearing response must be understood.

INTRODUCTION

Seismic isolation is used in many bridge applications to protect structural elements from the effects of strong-ground motion. High-damping rubber (HDR) bearings are one type of isolator commonly used in bridge design and retrofit, combining high vertical stiffness, low horizontal stiffness, and moderate energy dissipation in a single device. This behaviour has some advantages for earthquake protection, because under service conditions, such as wind or small earthquakes, the stiffness of the bearing is high, and the forces and deformation in the structure are expected to be in the elastic range. In a moderate seismic event, the bearing deforms, thus isolating the structure and providing additional energy dissipation. In an extreme earthquake loading, the strain-stiffening behaviour of the elastomer limits the deformation in the bearing, at the expense of increased force, which helps to reduce the risk of bearing instability.

[1] PhD candidate, European School for Advanced Studies in Reduction of Seismic Risk (ROSE School), Università degli Studi di Pavia, Via Ferrata 1, 27100 Pavia, Italy. Email: damian.grant@unipv.it
[2] Professor, University of California, Berkeley, USA. Email: fenves@ce.berkeley.edu
[3] Professor, Università degli Studi di Pavia, Pavia, Italy. Email: auricchio@unipv.it

The dynamic analysis of structures for seismic assessment and design requires an accurate mathematical model of the isolation bearings. The strongly nonlinear response of HDR bearings has made the development of mathematical models challenging. Unlike other isolation devices, such as lead–rubber bearings and friction bearings, a bilinear approximation to the force-deformation relationship is not adequate for HDR bearings under unidirectional or bidirectional loading [1]. In addition, laboratory tests [2, 3] reveal other characteristics of HDR bearings, including "scragging", Mullins' effect [4, 5], strain-induced anisotropy, and dependence on load history. Other factors that are difficult to represent are the variation in horizontal stiffness with axial load and temperature, strain-rate dependence and ageing effects.

To enable dynamic analysis of structures with HDR bearings, several mathematical models have been proposed in the literature for the unidirectional loading [6, 7]. In general, these models are adequate for describing bearing response under a restricted set of loading conditions, but commonly require the identification of a large number of material parameters with little obvious physical significance, and do not adequately describe degradation of bearing response over a series of tests [8].

Furthermore, there are currently no models available to describe the bidirectional shear force–displacement response of HDR bearings. Although current design guidelines for isolated bridge design [9] do not require bidirectional analysis, these recommendations are based on the response of seismically isolated buildings. Recent parametric studies by Huang [1] have shown that, for seismically isolated bridges, the response in the longitudinal and transverse horizontal directions may not be considered independently. For accurate time history analysis of bridges isolated with HDR bearings, a model developed specifically for bidirectional loading will be required.

Modelling issues aside, the nonlinear behaviour of HDR bearings may also lead to some difficulties in the design of piers in isolated bridges. Although pier yielding is utilised as a ductile failure mechanism in non-isolated bridges, existing design guidelines [9] for isolated bridges prescribe behaviour factors that correspond to elastic pier behaviour. For Lead–Rubber (LR) and Friction Pendulum™ System (FPS) bearings, the maximum force that may be transmitted through the bearing is relatively limited, which effectively limits the maximum bending moment developed in the piers. The stiffening behaviour of HDR bearings, however, implies that bearing and pier forces developed during a high intensity earthquake could be significantly more demanding than at the design level. Consequently, piers must be either designed elastically for overstrength loads, or detailed for ductile behaviour. In the latter case, the interaction between pier yielding and isolation needs to be studied, to verify the effectiveness of HDR bearings as an isolation system at high levels of input motion.

In this paper, a phenomenological model that effectively describes the bidirectional response of HDR bearings is presented. Using this model for bearings, time history analyses are carried out for a simple isolated bridge system, using real earthquake records scaled to different intensity levels. In this study, pier response is limited to elastic behaviour at all levels of intensity, and all energy dissipation is assumed to take place in the bearings. The results from these analyses are used to investigate the relationship between earthquake intensity and pier response for isolated and non-isolated bridge systems.

BIDIRECTIONAL MATHEMATICAL MODEL FOR HDR BEARINGS

A mathematical model has been developed which accurately describes the bidirectional, rate-independent behaviour of HDR bearings [8]. The model is able to describe the reduction in bearing stiffness due to "scragging" and Mullins' Effect [4, 5] under cyclic loading. By calibrating material parameters over a series of bidirectional tests, it has been shown that the model is able to represent, *a priori*, observed experimental response [8]. Furthermore, the model has also been extended to describe rate-dependent

behaviour [10]. A simplified, non-degrading version of the rate-independent model is summarised below, and is used to model bearing behaviour in the system analyses that follow.

The bidirectional behaviour of a bearing is expressed in terms of vector quantities **F**, **U** and **n**, representing the resisting force, deformation and normalised velocity:

$$\mathbf{F} = \begin{Bmatrix} F_x \\ F_y \end{Bmatrix} \qquad \mathbf{U} = \begin{Bmatrix} U_x \\ U_y \end{Bmatrix} \qquad \mathbf{n} = \frac{\dot{\mathbf{U}}}{\left\| \dot{\mathbf{U}} \right\|} \tag{1}$$

where the subscripts x and y refer to the components of a quantity in orthogonal directions in the plane of the bearing.

The resisting force vector is decomposed into elastic and hysteretic force, $\mathbf{F_1}$ and $\mathbf{F_2}$, and is defined by the following expression:

$$\mathbf{F}(\mathbf{U},\mathbf{n}) = \mathbf{F}_1(\mathbf{U}) + \mathbf{F}_2(\mathbf{U},\mathbf{n}) \tag{2}$$

The original presentation of the model [8] considered degradation of stiffness and damping response with a scalar damage parameter. Long-term and short-term degradation were accounted for separately, to allow calibration of model parameters across a series of bidirectional experimental tests. However, scragging and Mullins' effect are not considered in the simplified model presented here, as the focus is on a qualitative understanding of bearing overstrength, and not a quantitative study of changes in bearing properties with cyclic loading and time.

The resisting force described by Eq. (2) depends on the velocity vector only through its direction, **n**, and it is therefore independent of strain rate. Reference [10] introduced an additional force term that depends on the magnitude of the velocity, to account for strain-rate dependence in bearing behaviour. This extra component allows calibration of strain-rate dependent and strain-rate independent model parameters separately; in this paper, however, it will be assumed that any strain rate effects have been taken into account in terms $\mathbf{F_1}$ and $\mathbf{F_2}$.

Grant [8] showed that assuming a state of simple shear in the bearing, and a generalised Mooney–Rivlin strain energy function, the elastic force can be expressed as an odd fifth order polynomial function of the displacement:

$$\mathbf{F}_1 = \left(a_1 + a_2 \left\| \mathbf{U} \right\|^2 + a_3 \left\| \mathbf{U} \right\|^4 \right) \mathbf{U} \tag{3}$$

where a_1 to a_3 are material parameters.

The hysteretic force is obtained in a manner similar to bounding surface plasticity [11]. A bounding surface in force space is defined by the following pair of expressions:

$$B(\mathbf{U}) = \left\| \mathbf{F_2} \right\| - R(\mathbf{U}) = 0 \tag{4}$$

$$R(\mathbf{U}) = b_1 + b_2 \left\| \mathbf{U} \right\|^2 \tag{5}$$

where b_1 and b_2 are material parameters. Equations (4) and (5) describe a circular bounding surface in force space with a radius, R, which is a function of the displacement vector magnitude.

The position of the force vector relative to the bounding surface is described by a scalar distance variable, δ, and a unit direction vector along which the distance is measured, $\boldsymbol{\mu}$. Both terms are measured with respect to the 'image force', $\hat{\mathbf{F}}$, which performs a role analogous to the 'image stress' in bounding surface plasticity [11]. The image force is defined by projecting the unit normalised velocity vector, $\mathbf{n}$, from the origin onto the bounding surface:

$$\hat{\mathbf{F}} = R\,\mathbf{n} \tag{6}$$

The parameters δ and $\boldsymbol{\mu}$ are then taken as the magnitude and unit direction of the vector pointing from the current force point to the image force:

$$\delta = \left\| \hat{\mathbf{F}} - \mathbf{F}_2 \right\| \qquad \boldsymbol{\mu} = \frac{\hat{\mathbf{F}} - \mathbf{F}_2}{\left\| \hat{\mathbf{F}} - \mathbf{F}_2 \right\|} \tag{7}$$

Finally, to fully define the evolution of $\mathbf{F}_2$, a relationship is needed to describe both the direction and magnitude of the rate of change of hysteretic force, $\dot{\mathbf{F}}_2$. The hysteretic force is assumed to evolve towards the image force in $\mathbf{F}_2$ space, such that:

$$\frac{\dot{\mathbf{F}}_2}{\left\| \dot{\mathbf{F}}_2 \right\|} = \boldsymbol{\mu} \tag{8}$$

The magnitude of the change is given implicitly in terms of a scalar evolutionary equation for δ:

$$\dot{\delta} = -b_3\,\delta \left\| \dot{\mathbf{U}} \right\| \tag{9}$$

which describes a smooth transition from high to low values of δ, with a rate dictated by the material parameter, b_3. Although Eq. (9) is expressed in rate form, the appearance of time derivatives on both sides of the equation results in a rate-independent model.

Equations (6) and (7) may be rearranged to obtain the following expression for the hysteretic force:

$$\mathbf{F}_2 = R\,\mathbf{n} - \delta\,\boldsymbol{\mu} \tag{10}$$

The evolution of $\mathbf{F}_2$ is summarised in Figure 1. The smooth transition described by the scalar equation, (9), is illustrated for unidirectional loading in Figure 1b. For a given value of $\mathbf{U}$, the values of R and δ are determined, and from these, $\mathbf{F}_2$ is calculated. For bidirectional loading, Figure 1b shows the definition of the image force, and vectors $R\,\mathbf{n}$ and $\delta\,\boldsymbol{\mu}$, which are used to determine $\mathbf{F}_2$ from Eq. (10). Note that when δ is equal to zero, the hysteretic force is in the direction of the velocity vector, with $\mathbf{F}_2 = \hat{\mathbf{F}} = R\mathbf{n}$. For non-zero δ, $\mathbf{F}_2$ evolves to the image force in the direction of $\boldsymbol{\mu}$, as δ decreases according to Eqs. (9) and (10).

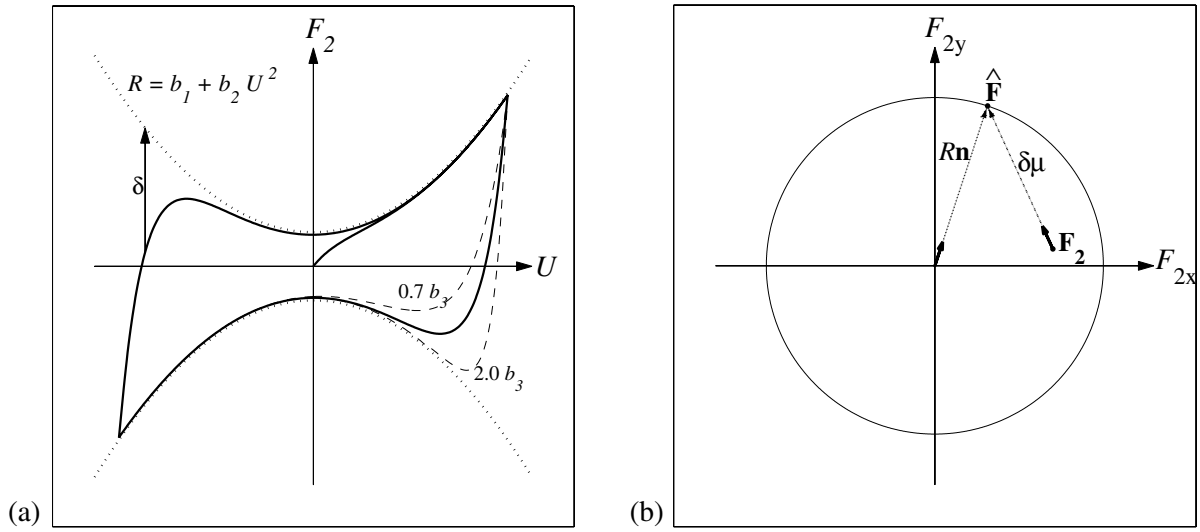

Figure 1. Hysteretic component of force. (a) Unidirectional and (b) bidirectional evolution.

ISOLATED BRIDGE STRUCTURAL MODEL

Bridge model

A number of bidirectional time history analyses of a simple isolated bridge model (shown in Figure 2) were carried out for a range of bearing model parameters, pier properties and ground motions. The longitudinal and transverse response of the bridge was represented by a four degree-of-freedom system, with the weight of the superstructure and pier concentrated above and below the isolation bearing system, respectively. The tributary superstructure weight used was 10000 kN, and the pier weight was 1000 kN. This simple model of bidirectional bridge response assumes that the bridge superstructure is rigid, and that all piers and bearings are identical.

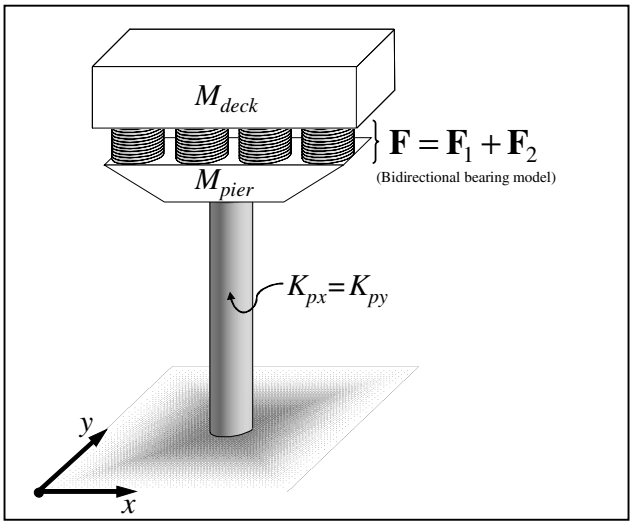

Figure 2. Four degree-of-freedom bridge model.

Elastic pier behaviour was assumed, and the longitudinal and transverse stiffnesses (K_{px} and K_{py}) were selected to provide a non-isolated fundamental period of 0.75 seconds in each direction, which gives values of $K_{px} = K_{py} = 71500$ kN/m. Although the stiffness of a pier is typically different in transverse and longitudinal loading, the assumption that $K_{px} = K_{py}$ describes the behaviour of bridge bents with a rigid

cap beam fully coupling transverse pier response, or piers with a moment of inertia significantly higher in the transverse direction. No viscous damping was used in the piers.

Bearing properties

The mathematical model discussed earlier was used to describe the bidirectional behaviour of the bearings. Due to the fact that no full scale, bidirectional test results were available for HDR bearings, data from tests of scaled bearings were used. The Caltrans Protective Systems Project at the University of California, Berkeley [1,2,3], included displacement-controlled tests on low-modulus, high-damping Bridgestone KL301 bearings. These bearings was originally specified as 2.5 scale bearings for building seismic isolation [5], with a diameter of 175 mm, and total rubber thickness (T_r) of 45 mm. However, bearings scaled by a factor of 4.0 are more appropriate for bridge applications.

The calibration of the mathematical model for the scaled Bridgestone bearings was described by Grant [8], including a full mathematical description of the degradation due to scragging and Mullins' effect. The virgin material parameter set was converted to SI units, and adjusted to allow for an initial scragging level of 250% shear strain. This initial scragging accounts for the fact that bearings are typically provided by the manufacturer in a degraded state, and subsequent hysteretic behaviour within this limit may be considered stable. The parameters were further adjusted to describe the total bearing system behaviour of four bearings per pier. Finally, the scaling factor to convert from scaled to prototype bearings, η, was used as a variable in the bearing design process described below. Parameters were scaled by assuming that shear stress–shear strain properties of the elastomer remain constant; forces were multiplied by η^2 and displacements were divided by η. Scaling the bearing size in all directions allows the first and second shape factors, S_1 and S_2, to be maintained. These are defined as [5]:

$$S_1 = \frac{\phi}{4t} \qquad\qquad S_2 = \frac{\phi}{T_r} \tag{11}$$

where ϕ is the diameter of the steel shim, t is the thickness of each rubber layer, and T_r is the total rubber thickness, as defined earlier. For the Bridgestone bearings considered in this paper, $S_1 = 20$ and $S_2 = 4$.

Ground motions

A set of ground motion records was selected from the FEMA/SAC database [12] to use as input for the time history analyses. The database contains several suites of ground motion, scaled to the United States Geological Survey (USGS) hazard maps for various seismic hazard zones and return periods. The records are provided in orthogonal pairs, and are rotated into fault normal (FN) and fault parallel (FP) components. Each pair of records is scaled by a single scaling factor to minimise the squared error between the USGS target spectrum and the average response spectrum of the time histories at periods of 0.3, 1.0, 2.0 and 4.0 seconds. A suite of earthquake recordings corresponding to a 10% exceedance-in-50-year hazard for firm soil sites in the Los Angeles (LA) area was selected for the time history analyses. The acceleration and displacement response spectra for each of the 20 records, derived for a viscous damping ratio of 9.2% (discussed below) are shown in Figure 3. The bold line in each plot is the average of all 20 spectra.

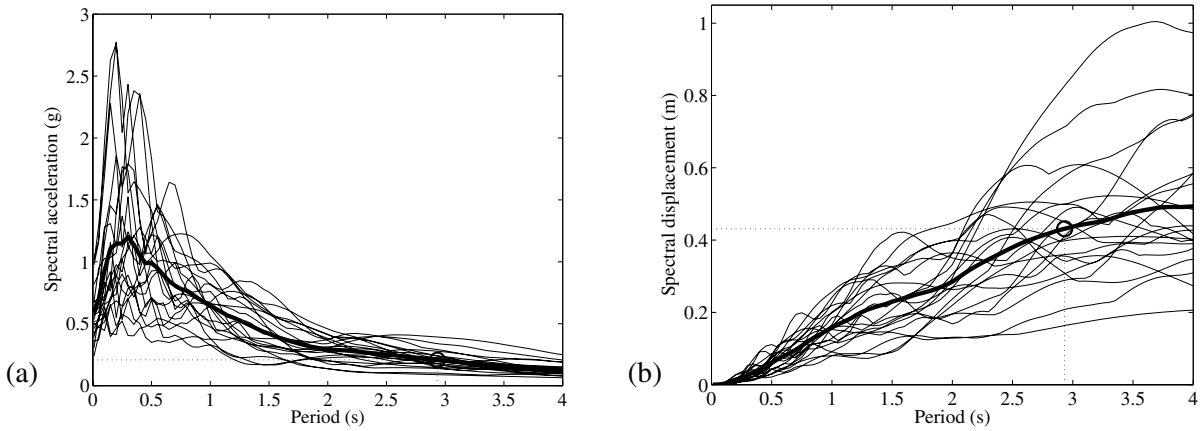

Figure 3. LA ground motion suite response spectra for 9.2% damping, and averaged spectra (bold), with displacement-based bearing design point (circled). (a) Acceleration and (b) displacement response spectra.

Bearing design

State-of-the-practice design codes [9] and design methods [13] recommend the use of an equivalent linear viscoelastic model for use in bearing design. Even more than other isolation devices, the effective stiffness (K_{eff}) and equivalent viscous damping (β_{eff}) for HDR bearings are strongly strain-dependent. The AASHTO specifications for isolation design prescribe a lateral displacement limit for elastomeric bearings of $2.5T_r$, in addition to limits for the total shear strain due to vertical loads, rotation and lateral displacement. Stanton [14] recommends a displacement limit of $2.0T_r$ to prevent delamination of the elastomer from the steel plates. Following this recommendation, a bearing design displacement corresponding to 200% design strain was considered in this paper. As the rubber thickness scales with the scaling factor, η, the bearing design displacement is given by:

$$U_d = (200\%)(45\text{mm}) \times \eta \tag{12}$$

The effective stiffness at the design level, $K_{eff,b}$, is calculated from the unscaled bearing parameters obtained earlier, and also increases in proportion to the scaling factor. The equivalent viscous damping, $\beta_{eff,b}$, is found by integrating the mathematical model (see Grant [10] for details) to obtain the area under the stabilised hysteresis loop, and is independent of scaling factor; a value of $\beta_{eff,b} = 9.8\%$ was calculated for the model parameters used here.

A displacement-based design procedure [13] was adopted to obtain a bearing size appropriate for the design level ground motions described above. The pier mass was ignored, and unidirectional ground motion was considered, resulting in a single degree of freedom system, with pier and bearing stiffness in series. The effective period, equivalent viscous damping and design displacement of the entire system, for no pier damping, can then be obtained from the following expressions:

$$T_{eff,sys} = 2\pi \sqrt{M_{deck}\left(\frac{1}{K_{eff,b}} + \frac{1}{K_{px}}\right)} \tag{13}$$

$$\beta_{eff,sys} = \frac{\beta_{eff,b} K_{px}}{K_{eff,b} + K_{px}} \tag{14}$$

$$U_{sys} = U_d + U_p = \left(1 + \frac{K_{eff,b}}{K_{px}}\right) U_d \tag{15}$$

where U_p is the displacement of the pier.

The average displacement spectrum over all the 20 time histories in the LA suite was used for design, calculated at a damping level of $\beta_{eff,sys}$. The length scaling factor, η, was used as the design parameter, representing the size of the bearing. A trial scaling factor was assumed, and the structural period corresponding to a displacement of U_{sys} was found from the design spectrum. The scaling factor was adjusted until the period was approximately equal to the effective period of the system, $T_{eff,sys}$.

The above procedure converged for a scaling factor of η = 4.4, which corresponds to a prototype bearing diameter of 770 mm and rubber thickness of 200 mm. The design point is illustrated on Figure 3b – the displacement response spectrum for $\beta_{eff,sys}$ = 9.2% damping. Other system design parameters, and scaled bearing model parameters, are given in Table 1. The unidirectional bearing model response under cycles of 100%, 200% and 250% strain is shown in Figure 4a.

Table 1. Bridge model system properties, and parameters for design bearing system (η = 4.4).

$K_{eff,b}$	U_d	$T_{eff,sys}$	U_{sys}	a_1	a_2	a_3	b_1	b_2	b_3
5130 kN/m	400 mm	2.9 sec	430 mm	3510 kN/m	-3720 kN/m^3	10200 kN/m^5	258 kN	3270 kN/m^2	16.9 /m

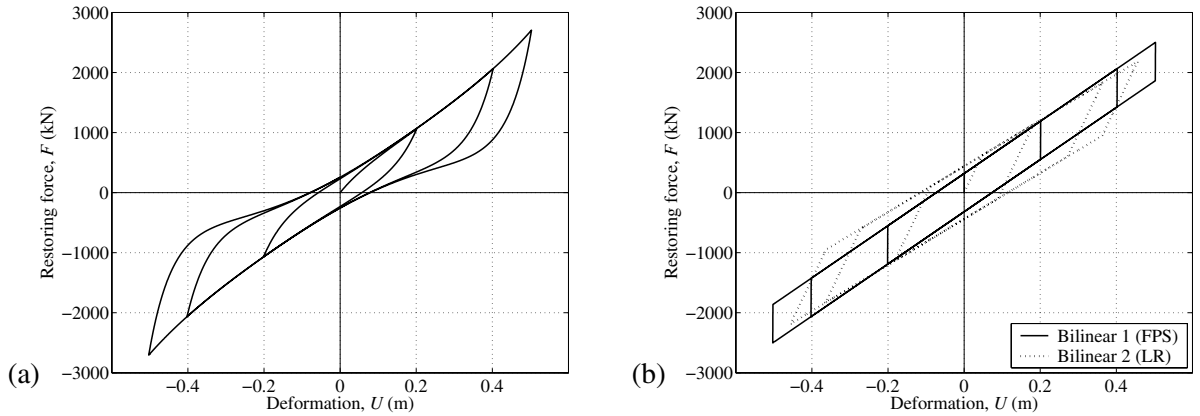

Figure 4. Unidirectional response of bearing models for 50%, 100% and 125% of design displacement. (a) HDR bearing model, and (b) bilinear model.

ANALYSIS RESULTS AND DISCUSSION

Time history analyses

The four degree-of-freedom bridge model, with properties described above, was subjected to the LA suite of ground motions. FN and FP records were applied simultaneously in orthogonal directions to determine the bidirectional response of the bridge. Newmark's method [15] with parameters β = 0.25 and γ = 0.5 was used for the solution of the equation of motion, and the nonlinear state determination was carried out with Newton–Raphson iteration. The tangent stiffness matrix appropriate for the bearing model is given by Grant [10].

A series of analyses was carried out with ground motion scaling factors ranging from 0.05 to 1.5, in addition to the scaling factors already applied in the preparation of the FEMA/SAC database. The range of ground motion scaling factors is used to investigate the sensitivity of bearing displacement and pier force to ground motion intensity. A ground motion scaling factor of 1.0 corresponds to the design level intensity (I_d), as the average of the unscaled ground motion displacement spectra was used for the bearing design. This allows the ground motion scaling factor to be described as a normalised intensity level, I/I_d, with $I/I_d < 1$ corresponding to less-than-design intensity, and $I/I_d > 1$ corresponding to greater-than-design intensity.

For each bidirectional analysis, the peak bearing displacement and pier force were determined from the vector magnitudes at each time step. These maxima were normalised with the bearing design displacement, U_d, and design force, $F_d = K_{eff,b}U_d$, and are shown over the range of intensities in Figure 5. The mean of the maxima across the whole ground motion suite is shown in bold in each plot. Although there is significant scatter in the individual ground motion results, some general trends can be observed. At the design intensity level ($I/I_d = 1$), the peak displacements and forces generally exceed the design values, and the mean response is 30% higher in displacement and 50% higher in force. The primary reason for this unconservatism is that an average of all 20 ground motion records was used for design, but the bidirectional analysis effectively selected the maximum direction from each pair. This observation was also made by Huang [1] from a larger series of parametric studies, and it was suggested that a nonlinear response spectrum which gives the maximum response in any direction would be a useful design aid.

Figure 5 also illustrates the effect that the HDR bearing strain-stiffening phenomenon has on seismic isolation. For displacement levels in excess of the design displacement, Figure 5a shows that bearing deformation does not increase in direct proportion to the intensity. However, Figure 5b illustrates the trade-off of limiting the displacement; the pier forces are increased significantly for the higher intensity levels. These observations will be more evident in the next section when the strain stiffening HDR model is compared with a bilinear model typical of other bearing types.

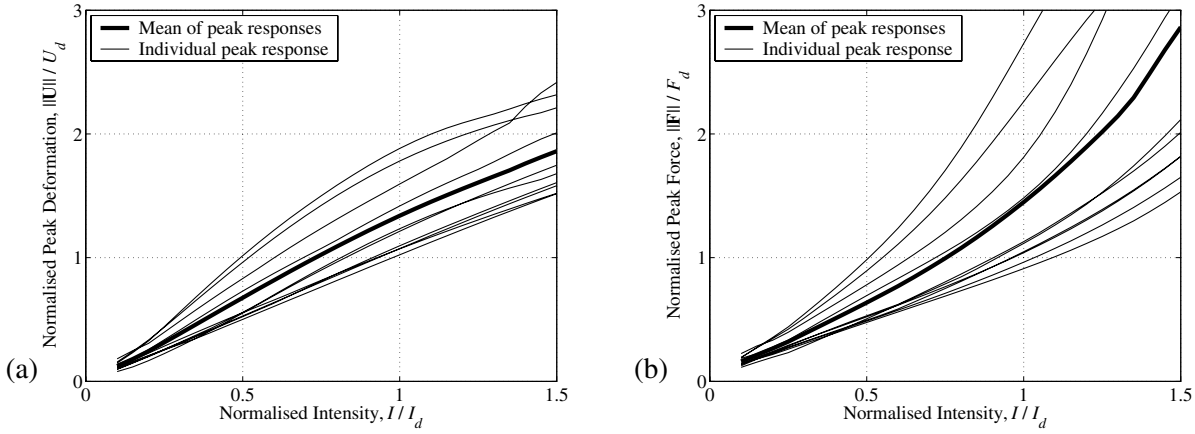

Figure 5. Variation in maximum response with intensity for LA ground motion suite. (a) Bearing displacement and (b) pier force.

Sensitivity study: bearing type

To compare the effectiveness of HDR isolation systems with LR and FPS systems, another set of analyses was carried out with a bilinear force–displacement model for the bearings. The bidirectional response was characterised by a classical plasticity approach with a kinematic hardening yield surface. The model is completely defined by three parameters: the zero-displacement force intercept (Q_D), and the elastic and post-yield stiffnesses (K_1 and K_2, respectively). This model has been shown to describe bidirectional response of FPS bearings [16] effectively, and is also commonly applied to LR bearings. In the latter case,

model parameters are strain-dependent, at least for the lead core dimensions considered by Huang [1]. Furthermore, the bidirectional behaviour of LR bearings is not completely described by the classical kinematic hardening approach for all load paths. These limitations notwithstanding, the bilinear model was adopted to contrast the behaviour of softening isolation devices such as FPS and LR bearings, with the stiffening behaviour of HDR bearings at high strains.

Two separate sets of bearing parameters were selected, and the time history analyses described above were carried out. The first parameter set was determined by setting $K_{eff,b}$ and $\beta_{eff,b}$ as identical to the HDR case, and solving for the three bilinear model parameters. A pseudo-yield displacement of 0.01 inches (0.25 mm) was chosen, as recommended by Constantinou [17] for FPS bearings. The bearing design displacement was again set at 400 mm, which results in the same design point identified in Figure 3b.

The second bilinear parameter set was determined by scaling parameters calibrated for scale LR bearings by Huang [1]. The bearings were originally 180 mm in diameter, with a total rubber thickness of 87 mm. An isolation system of four bearings, with a scaling factor of 4.2, was used to obtain a design point for the LA suite averaged displacement response spectrum, corresponding to a design displacement of U_d = (100%)T_r = 365 mm. At this design level, the effective stiffness of the bearing system was 5030 kN/m, and the equivalent viscous damping was 12.4%. The unidirectional force–displacement behaviour for each bilinear model is shown for 50%, 100% and 125% of the bearing design displacement in Figure 4b.

The average maxima over all records are shown in Figure 6. The response quantities from each bearing model are normalised with the design displacement and design force of each bearing so that the results can be compared. The bearing models have been designed for the design intensity individually, and the displacement and force response is approximately the same at the design level of the bearing ($U/U_d = F/F_d$ = 1). However, because of the unconservatism at the design ground motion scaling factor, I/I_d = 1, displacements and forces for the bilinear model have already diverged from the HDR stiffening model at this level of intensity. For intensity levels above I_d, the difference between stiffening and bilinear response continues to diverge. This again illustrates the trade-off discussed earlier – the stiffening behaviour of HDR bearings limits the maximum displacements for high strain levels, at the cost of higher forces developing in the piers. The difference between the two bilinear models is relatively small, although the FPS bilinear parameter set is slightly more effective at limiting displacement than the LR model.

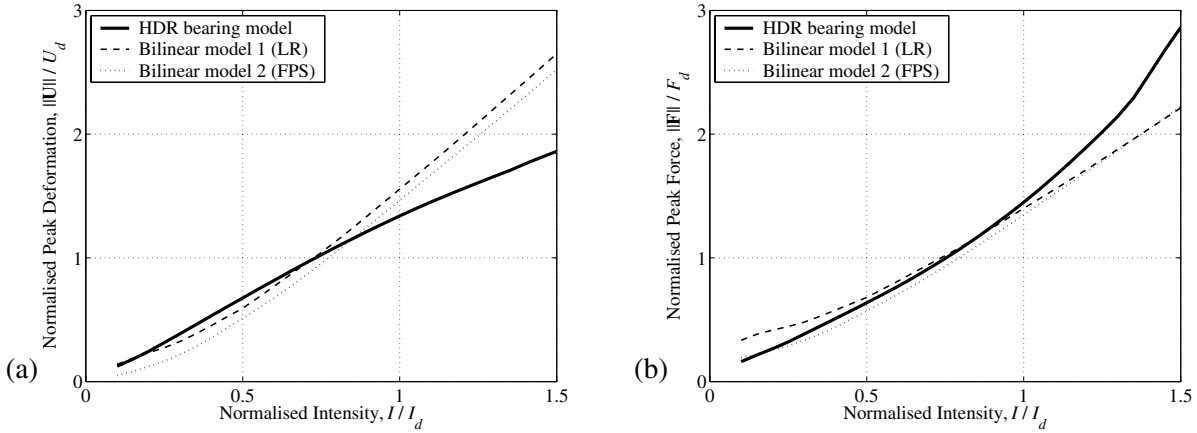

Figure 6. Variation in mean maximum response with intensity for different bearing models. Bilinear models designed in a similar manner to HDR model, and represent LR and FPS bearing response. (a) Bearing displacement and (b) pier force.

Sensitivity study: scragging

A second sensitivity study was carried out on the inclusion of the scragging phenomenon in the bearing model. The model presented by Grant [8] was used to model the first-cycle degradation in bidirectional HDR bearing response. A scalar scragging parameter is used which is set at the maximum displacement vector magnitude experienced by the bearing. When the displacement exceeds this value, the scragging parameter increases, and both elastic and damping forces in the model are reduced for subsequent loading. Model parameters accounting for the scragging effect were retained from the original calibration [8], adjusted for the scaling factor, η, and included in the time history analysis. Furthermore, another two sets of analyses were carried out with virgin material properties, including and excluding scragging effects, to investigate the effect on bridge response if the original bearing properties are recovered.

The results from this set of analyses are summarised in Figure 7. The inclusion of scragging in the model clearly results in much larger peak displacements, whether the initial parameter set corresponds to virgin or pre-scragged response. These results should be interpreted with caution: the scragging model was only calibrated for shear strains up to 350%. The sharp increase in gradient in Figure 7a suggests that, at higher intensity levels, the first large displacement excursion reduces the stiffness of the bearing excessively, and the modelling of subsequent cycles may not be realistic. It can also be observed that, for the prescragged models, the response does not begin to diverge until the prescragging level of 250% strain ($U = 1.25U_d$) is exceeded, due to the isotropic softening model used for the degradation. The virgin parameter set with no scragging results in a slightly stiffer model, and this is reflected in the lower displacements in Figure 7a. The forces for the four models, shown in Figure 7b, are not significantly different across the intensity range. The models with virgin properties exhibit slightly higher forces for the mid-range of intensities, and the inclusion of scragging in the analysis has little effect on forces, except for at the highest ground motion scaling factors considered.

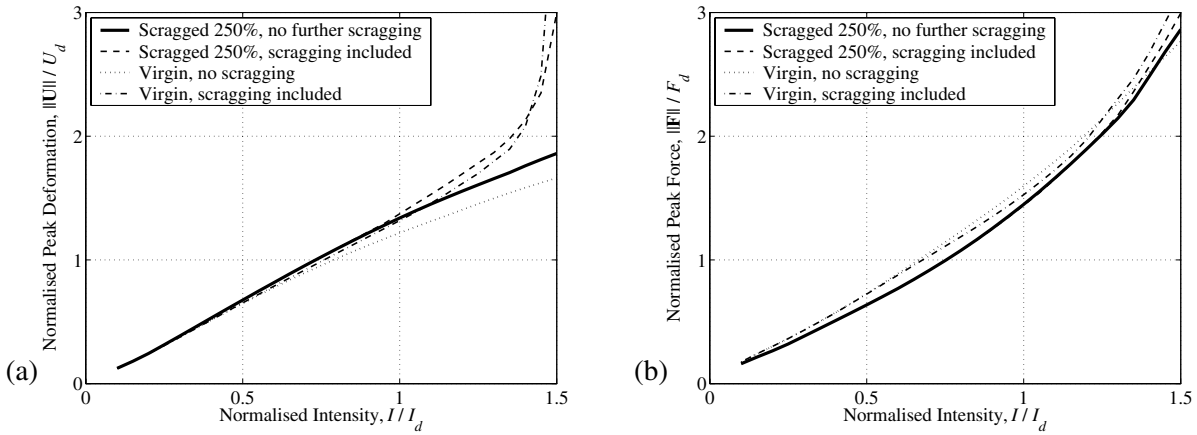

Figure 7. Variation in mean maximum response with intensity for different scragging considerations. (a) Bearing displacement and (b) pier force.

Sensitivity study: ground motions

The use of a different ground motion set for the bearing design and time history analyses was also investigated. Ten pairs of near-fault (NF) ground motion records from the FEMA/SAC database [12] were used, and the bearing was redesigned for the mean displacement spectrum of all 20 records. Near-fault ground motions are considered to be particularly demanding for isolated systems, due to the high spectral response at long periods, and high amplitude velocity pulses. The NF recordings in the FEMA/SAC database are not scaled to a design spectrum, and consequently there is significantly more scatter in the response spectra. The design procedure resulted in a bearing scaling factor of 5.4, with U_d = 490 mm and $K_{eff,b}$ = 6300 kN/m.

The displacement and force response, normalised separately with respect to the values for each bearing design, are shown in Figure 8. It can be observed that the NF records are more demanding for the isolated system, even when the isolators have been designed for the averaged response spectrum of the records. The primary reason for this discrepancy could be that the FN components of near-fault recordings are generally much more demanding at long periods than the FP components. The structure has been designed for the average of all the motions, but it is the FN component which is principally responsible for the peak response. This observation was also used to explain the unconservatism of design for the LA records, although in this case the difference between FN and FP components is not as significant, and the averaged response spectrum is better at representing the average demand. In any case, a design procedure which properly takes into account this increase in demand is particularly important for isolation design in near-fault regions.

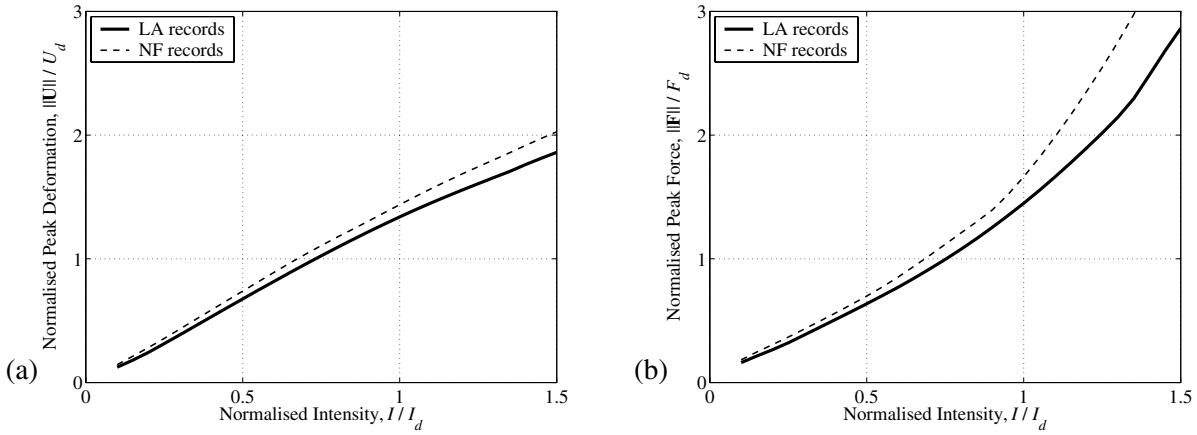

Figure 8. Variation in mean maximum response with intensity for LA and NF ground motion suites. Bearings designed separately for mean displacement spectrum of each suite. (a) Bearing displacement and (b) pier force.

Sensitivity study: unidirectional vs. bidirectional analyses

Bidirectional analyses require extra modelling and computational effort on the part of the analyst. Ground motions are typically applied in orthogonal directions in independent, unidirectional analyses, and the maximum response is considered for design. To determine if such a procedure accurately captures the real peak response, the analyses were repeated with ground motion pairs from the LA suite, applied independently. The maximum displacement and force were calculated for each pair of records, and averaged over the suite. In addition, the mean of all 20 unidirectional analyses was computed for each response quantity, to investigate the unconservatism in the design approach that was observed earlier.

The results from this study are summarised in Figure 9. The maximum displacements, averaged over all ground motion pairs, do not significantly underestimate the bidirectional displacements and forces across the range of intensities. This suggests that unidirectional analyses could be adequate for isolated bridge design; however, the bridge model used here is an idealisation of real bridges, and this may not apply for bridges with different stiffness in transverse and longitudinal directions. In addition, the ground motion pairs in the LA suite had been rotated into FN and FP components, which may orient the unidirectional analyses with the direction of maximum demand.

The means of response quantities calculated from unidirectional analyses are significantly lower than the maxima from each ground motion pair, as predicted earlier. The displacements and forces at design intensity are very close to the design values, which suggests that the design procedure described earlier is

adequate, provided that the displacement design spectrum represents the direction of maximum earthquake demand.

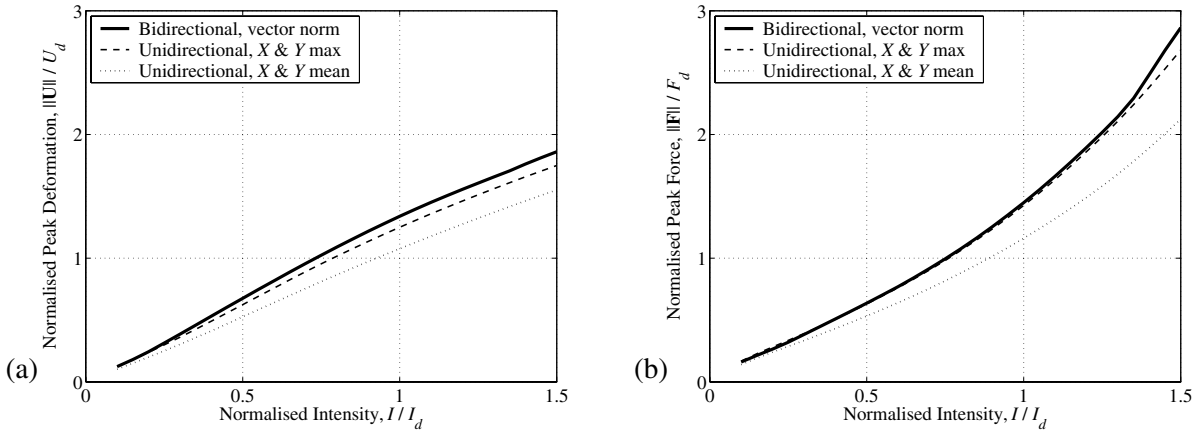

Figure 9. Variation in mean maximum response with intensity for bidirectional and unidirectional loading combinations. (a) Bearing displacement and (b) pier force.

Sensitivity study: pier flexibility

A final sensitivity study was carried out considering different pier stiffnesses. Non-isolated pier periods of 0.75, 1.0 and 1.5 seconds were used, corresponding to pier stiffnesses of 71500, 40200 and 17900 kN/m, respectively, considering only the superstructure mass in the calculation. Figure 10 shows that the series system behaviour is insensitive to the pier stiffness, as the flexibility of the bearing dominates the response. Of more interest for flexible bridges is how effective seismic isolation can be at reducing the demand. The data in Figure 10 could be compared with a non-isolated, elastic pier analysis, although this would require a more realistic representation of damping in the pier.

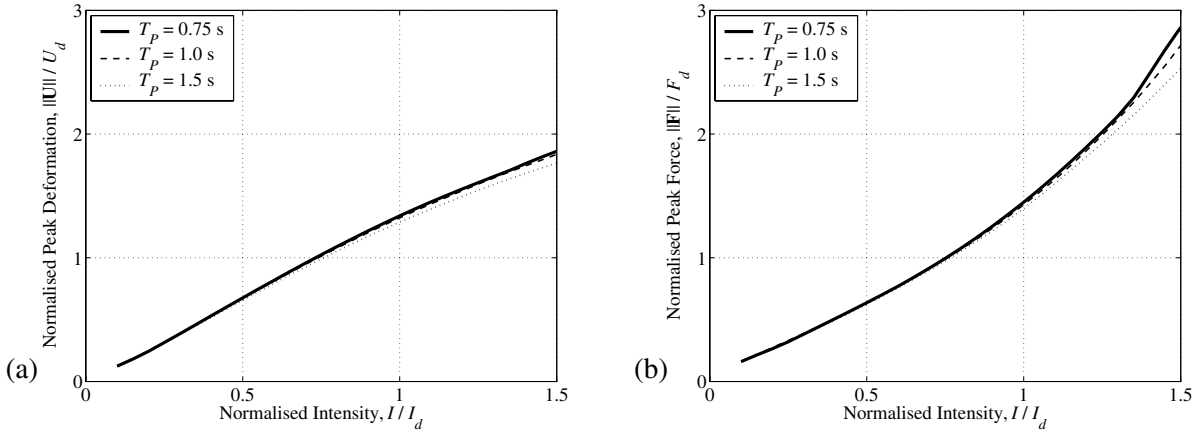

Figure 10. Variation in mean maximum response with intensity for different pier flexibilities. (a) Bearing displacement and (b) pier force.

CONCLUSIONS

HDR bearing behaviour is characterised by strain stiffening behaviour and nonlinear damping, and is particularly difficult to model under bidirectional loading conditions. The lack of adequate models has made it difficult to verify the effectiveness of HDR bearings as an isolation system for bridges under high intensity ground motion input. The stiffening behaviour of the bearings, while limiting bearing

displacements, could be expected to result in excessive moment demands on piers if the design level intensity is exceeded.

In this paper, a mathematical model of HDR bearing bidirectional behaviour was presented, and used in a series of analyses of a simple isolated bridge model. A range of scaling factors was applied to real earthquake records, to investigate the overstrength demand for ground motion intensity in excess of the design level. In addition, several variations of the analysis were performed, to investigate the sensitivity of the results to the modelling assumptions.

A number of conclusions can be drawn from the study. The strain stiffening behaviour of HDR bearings limits the bearing displacements for scaling factors greater than the design level, but forces in the piers may be significantly greater than designed for. If piers are not detailed for this extra demand, there is a potential conflict with capacity design philosophy, which aims to desensitise the risk of structural collapse to the intensity of the ground motion. By comparison, the displacement demand of LR and FPS bearings increases more steeply with intensity, although the pier forces are more controlled. Provided this extra displacement demand can be accommodated, the risk of overloading the structure is lower.

The suggestion of Huang [1], that a response spectrum used for design should represent the maximum demand in all directions, was also confirmed. This was shown to be especially important for near-fault recordings, for which the fault normal component is particularly dominant, and is known to be demanding for isolated structures. If such a response spectrum were available, the maximum demand from orthogonal unidirectional analyses could accurately describe the bidirectional structural demand.

The use of virgin or scragged bearing properties did not have a significant effect on the analysis results. When scragging was accounted for, the displacement demand was excessively large for high intensity input motion, although the extreme results were outside of the range of applicability of the scragging model. The sensitivity of the results to changes in pier stiffness was also low, as the bearing flexibility dominated the response of the series system. However, for systems with flexible piers, the possible reduction of demand through seismic isolation is lower.

The results of this study suggest that bridge designers should be aware of the potentially high demand on piers isolated with HDR bearings for extremes of ground motion, and that they should detail members accordingly. Alternatively, the option of using pier yielding in conjunction with isolation could be further investigated.

REFERENCES

1. Huang W-H. “Bi-directional testing, modeling, and system response of seismically isolated bridges.” PhD Thesis, University of California, Berkeley, 2002.
2. Thompson ACT. “High damping rubber seismic isolation bearings – behaviour and design implications.” CE299 Report, University of California, Berkeley, 1998.
3. Morgan TA. “Characterization and seismic performance of high-damping rubber isolation bearings.” CE299 Report, University of California, Berkeley, 2000.
4. Mullins TA. “Softening of rubber by deformation.” Rubber Chemistry and Technology 1969; 42(1): 339-362.
5. Clark P, Aiken ID, Kelly JM. “Experimental studies of the ultimate behavior of seismically-isolated structures.” Technical Report UCB/EERC-97/18. Berkeley:Earthquake Engineering Research Center, 1997.
6. Kikuchi M, Aiken ID. “An analytical hysteresis model for elastomeric seismic isolation bearings.” Earthquake Engineering and Structural Dynamics 1997; 26: 215–231.

7. Hwang JS, Wu JD, Pan T-C, Yang G. “A mathematical hysteretic model for elastomeric isolation bearings.” Earthquake Engineering and Structural Dynamics 2002; 31: 771–789.
8. Grant DN, Fenves GL, Whittaker AS. “Bidirectional modelling of high-damping rubber bearings.” Journal of Earthquake Engineering 2004; 8(Special Issue 1).
9. American Association of State Highway and Transportation Officials (AASHTO). “Guide specifications for seismic isolation design.” Washington:AAHSTO, 1999.
10. Grant DN. “Bridge isolation with high-damping rubber bearings – analytical modelling and system response.” PhD Thesis, Università degli Studi di Pavia, 2004.
11. Dafalias YF, Popov EP. “A model for nonlinearly hardening materials for complex loading.” Acta Mechanica 1975; 21(3): 173-192.
12. Woodward-Clyde Federal Services. “Suites of ground motion for analysis of steel moment frame structures.” Report No. SAC/BD-97/03, SAC Steel Project, 1997.
13. Priestley MJN, Seible F, Calvi GM. “Seismic design and retrofit of bridges.” New York:John Wiley & Sons, 1996.
14. Stanton J. “The 1997 AASHTO seismic isolation guide specification.” Proceedings of the U.S.–Italy Workshop on Seismic Protective Systems for Bridges, Technical Report MCEER-98-0015. Buffalo:Multidisciplinary Center for Earthquake Engineering Research, 1998.
15. Chopra AK. “Dynamics of structures: theory and applications to earthquake engineering.” Second Edition. New Jersey:Prentice Hall, 2001.
16. Mosqueda G. “Experimental and analytical studies of the Friction Pendulum System for the seismic protection of bridges.” CE299 Report, University of California, Berkeley, 2001.
17. Constantinou MC, Tsopelas P, Kim Y-S, Okamoto S. “NCEER–Taisei Corporation research program on sliding seismic isolation systems for bridges: experimental and analytical study of a Friction Pendulum System (FPS).” Technical Report NCEER-93-0020, Buffalo:National Center for Earthquake Engineering Research, 1993.